

This work has been submitted to the IEEE for possible publication. Copyright may be transferred without notice, after which this version may no longer be accessible

TRANSCENDING CONVENTIONAL BIOMETRY FRONTIERS: DIFFUSIVE DYNAMICS PPG BIOMETRY

A PREPRINT

Javier de Pedro-Carracedo*

Departamento de Tecnología Fotónica y Bioingeniería
Universidad Politécnica de Madrid (UPM)
Madrid, 28040 Spain
javier.depedro@uah.es

David Fuentes-Jimenez

Department of Electronics
University of Alcalá (UAH)
Alcalá de Henares (Madrid), 28871 Spain
david.fuentes@depeca.uah.es

Ana M. Ugena

Departamento de Matemática aplicada a las Tecnologías de la Información
Universidad Politécnica de Madrid (UPM)
Madrid, 28040 Spain
anamaria.ugena@upm.es

Ana P. Gonzalez-Marcos

Departamento de Tecnología Fotónica y Bioingeniería
Universidad Politécnica de Madrid (UPM)
Madrid, 28040 Spain
anapilar.gonzalez@upm.es

April 12, 2022

ABSTRACT

In the first half of the 20th century, a first pulse oximeter was available to measure blood flow changes in the peripheral vascular net. However, it was not until recent times the PhotoPlethysmoGraphic (PPG) signal used to monitor many physiological parameters in clinical environments. Over the last decade, its use has extended to the area of biometrics, with different methods that allow the extraction of characteristic features of each individual from the PPG signal morphology, highly varying with time and the physical states of the subject. In this paper, we present a novel PPG-based biometric authentication system based on convolutional neural networks. Contrary to previous approaches, our method extracts the PPG signal's biometric characteristics from its diffusive dynamics, characterized by geometric patterns image in the (p, q) -planes specific to the 0–1 test. The diffusive dynamics of the PPG signal are strongly dependent on the vascular bed's biostructure, which is unique to each individual, and highly stable over time and other psychosomatic conditions. Besides its robustness, our biometric method is anti-spoofing, given the convoluted nature of the blood network. Our biometric authentication system reaches very low Equal Error Rates (ERRs) with a single attempt, making it possible, by the very nature of the envisaged solution, to implement it in miniature components easily integrated into wearable biometric systems.

Keywords Biometric system · CNN architecture · 0–1 test · PPG signal dynamic · Pattern analysis

*Current address: University of Alcalá (UAH), Computer Engineering Department, Alcalá de Henares (Madrid), 28871 Spain.

1 Introduction

The relentless outbreak of the pandemic in our lives has put the globalized world in check. Paralysis to which economies across globe drive has been reversed, in many cases, by the spread of a latent wave for decades: digitization society. Life will condition by new technologies, an entire online ecosystem whose real repercussion is still a pipe dream even among those experts who venture timidly with hasty forecasts.

The health crisis has perpetrated a double recession, the economic and the social. With intermittent confinements expected shortly, the home has become our vital refuge due to the repetitive recurrence of the virus. Our interface with society relies entirely on technology. The introduction of digital processes has precipitated so that from our house, we have virtual access to a whole range of services that, until now, we were enjoying in person, for example, teleworking and online training. The digital assets of companies focus their efforts on the cloud in businesses, and factories are automated, e-commerce is growing unstopably, the virus being the catalyst for this dynamic.

In this vast digital spectrum looming, with the presumable paradigm shift, the global opening towards a fully digital world is imminent. In this time of transformation, structural reforms are peremptory. The role that technology will play in future societies is unquestionable. Virtually everything will connect to everything. However, this profound metamorphosis carries challenges that digital platforms themselves have to face. One of them is to keep the identities of the users of the different services protected, that is, to avoid identity theft so that it can unequivocally verify that a user is whom they say they are and not an impostor intruder with clearly fraudulent purposes. Today, the most secure authentication mechanisms are base on biometric methods. Compared to the traditional use of access passwords, the different biometric identification

In this vast digital spectrum looming, with the presumable paradigm shift, the global opening towards a fully digital world is imminent. In this time of transformation, structural reforms are peremptory. The role that technology will play in future societies is unquestionable. Virtually everything will connect to everything. However, this profound metamorphosis carries challenges that digital platforms themselves have to face. One of them is to keep the identities of the users of the different services protected, that is, to avoid identity theft so that it can unequivocally verify that a user is whom they say they are and not an impostor intruder with clearly fraudulent purposes. Today, the most secure authentication mechanisms are base on biometric methods. Compared to the traditional use of access passwords, the different biometric identification systems are very reliable and free the user from memorizing numerous keys [1]. The only access password lies in the user's anatomical characteristic, supposedly exclusive and non-transferable, whose emulation is extremely problematic even for the most seasoned intruders. Face, voice, iris, palm, and finger recognition are already a reality that safeguards socioeconomic transactions. The standard criteria that conventionally met to consider the relevance of a biometric access control system obey [2]:

- Cost of the biometric validation device.
- Biometric verification speed.
- Size of the biometric fingerprint that identifies a user.
- Degree of acceptance by the user.
- User comfort.
- Ease of maintenance.
- Unlinking of police records that may compromise the legal security of the individual.

The escalating technology that Big Data has undergone is a direct consequence of the instrumental ease with which one can acquire enormous data. In the clinical field, public databases are already available with thousands of physiological samples from healthy individuals and with various pathologies for different age ranges. In this sense, new technological solutions are gradually betting on biological signals that implicitly reveal distinctive anatomical characteristics of each subject, since they record the imprint of the organic systems that intervene in their generation.

Unlike morphological measurements, mostly dependent on the individual's skill in handling the biometric information capture device and highly sensitive to involuntary morphological disturbances, see, for example, a cut on the fingertip undergoes a fingerprint analysis—biological signals are not particularly affected by the individual's blunder and lend themselves to a more comprehensive biometric examination. The exploration of biometric characteristics includes morphological details of the waveform of the biological signal and dynamic peculiarities by the expected functional response of the physiological system of interest.

In the last decades, a preliminary diagnostic examination of the health status of an individual has been entrusted on many occasions to monitoring, using non-invasive methods, and the pertinent clinical analysis of biological signals generated by the human body [3]. Among the different biological signals that are usually measured today, one, particularly,

deserves special consideration, the PPG signal. The PPG signal reproduces the changes in blood volume that occur in the peripheral microcirculation [1]. The electro-optical technique that allows measuring these volumetric variations calls photoplethysmography (PPG) [4].

Since Alrick Hertzman, an American physiologist, devised the first photoelectric photoplethysmograph in 1937 [5], although rudimentary, recent technological advances provide devices, as modern pulse oximeters, increasingly smaller, lighter, and with a marked tendency to market themselves as wireless devices at a very affordable price [6, 7]. An essential aspect of the PPG technique lies in its low sensitivity to the location of the sensors, which gives versatility to photoplethysmography for its application in many areas, such as health, sports, or agri-food industry. Appearance due to the electronic simplicity, the cost-benefit ratio, the ease of signal acquisition, and, mainly, due to its non-invasive character [8, 9, 10]. Unlike other biological signals that require bulky measurement equipment, or even accessories, such as the use of gels (EEG) or electrodes (ECG), the PPG signal requires quite modest electronics. Electronics and optoelectronics uncomplicated, favor the construction of small pulse oximeters, easily integrable into smart devices [11]. A pulse oximeter consists of a light emitter and a photodetector. The photodetector collects and records the loss—dispersion and absorption—(pulse signal or PPG) that a light beam undergoes when it passes through or reflects in human tissue [12].

The PPG signal is widely used in clinical settings to monitor physiological parameters related to the cardiorespiratory system [13]. The PPG signal is complex. It composes an AC component—peripheral pulse synchronizes to each heartbeat—; and a quasi-DC part that varies slowly, due to respiration, vasomotor activity, and vasoconstrictor waves [14]. The mutual coupling between the different components is intricate and operates at different timescales to regulate blood volume based on physiological needs.

In this work, we use the PPG signal dynamics as a biometric reference of any individual. In this sense, we focus our attention on the geometric distribution of the PPG signal’s diffusive behavior, according to the (p, q) -plane proposed by the 0–1 test [15, 16, 17]. We believe that the PPG signal’s diffusive dynamics are unique to each individual since the diffusion constant of blood flow is subject to the structural configuration with which each individual has been endowed. A whole complex network of arteries, arterioles, and capillaries transports blood from the heart to the rest of the body thanks to the driving force exerted by the heart and synchronized with the respiratory rhythm. Although variations in the diffusive dynamics of the PPG signal can indeed hide point or progressive pathological abnormalities, such as, for example, physiological deterioration as a result of aging, specific congenital characteristics remain practically unchanged. In this regard, the blood dynamics (hemodynamics) in the peripheral capillary branching stand as ideal candidates for identifying the biometric pattern of an individual.

In this work, we use the PPG signals from 40 students, between 18 and 30 years old and non-regular consumers of psychotropic substances, alcohol or tobacco, selected to participate in a national research study [18, 19]. All signals were captured from the middle finger of the left hand and sampled at a frequency of 250 Hz [18], say, sampling time $\Delta t = 4$ ms. In this experimental setting, the PPG signals capture the blood microcirculation and are a true reflection of the peripheral capillary branching that each individual presents.

The credentials of each subject, their identity, are collected in blood flow dynamics through the peripheral capillary network. Its falsification is very difficult because of the intricacy of the capillary network, and complexity, which involves the same blood flow driven by the cardiorespiratory system. Furthermore, significant detail is that any biometric system based on the verification of the diffusive dynamics of the PPG signal requires the individual’s vital integrity. Someone, not without a negligible effort, could imitate the particular capillary morphology of an artificial finger. Still, it would be practically impossible to reproduce the diffusive dynamics that blood flow undergoes when circulating through that capillary structure, given the contribution of a multitude of subsystems that do not linearly make up the cardiovascular system.

Our proposal involves the recognition of dynamic patterns that characterize the diffusive behavior of the PPG signal. As an authentication mechanism [1], the biometric architecture consists of two stages: in a first phase, *enrollment phase*, 12 s of PPG signal are acquired from each individual using a pulse oximeter. These signal fractions are pre-processing to obtain several (p, q) -planes representative of each subject, the biometric pattern. From these (p, q) -planes, the neural network extracts 51,200 characteristics that encapsulate each individual’s biometric pattern and conveniently stored in memory. Afterward, *verification phase*, 12 s of PPG signal acquire from anyone who wishes to verify their identity, proceeding to their pre-processing and, through a classifier, to their comparison with the rest of the registered biometric patterns, to authenticate the identity of the user requesting it.

The rest of this paper is organized as follows. Section 2 condenses the advances made in the application of the PPG signal as a biometric marker over the past few years. Section 3 describes the theoretical foundation, in the mathematical framework of the 0–1 test, that underpins the biometric potential of the geometric patterns traced by the diffusive behavior of the PPG signal. In section 4 our novel proposal for a biometric classifier based on convolutional neural

networks is explained in detail. Section 5 shows the obtained results, both graphically and numerically, for various experimental settings. Also, in this section we analyze and interpret the obtained results. Finally, in section 5, we shortly outline the conclusions drawn from this study, which in turn serve as the basis for future work.

2 State of the art

The development of biometrics during the 20th century, according to its definition in [20]: “Measurable physical characteristics or personal behavioral traits used to identify or verify the identity of an individual”, began by conforming to the old paradigm of facial recognition and of fingerprints. Nevertheless, continued progress in the area of image processing and analysis has fostered the exploration of more sophisticated biometric system designs [21, 22] (for a sound review of classical biometric approaches and their evolution over time you are referred to [23]).

So far, in the 21st century, the development of biometric pattern recognition systems has evolved enormously, broadening its application spectrum in the context of morphological analysis, as reflected between the proposal of the anatomical characterization of the hand geometry in [2] and the made by [24] concerning 3D palmprint modeling. The same is true for other biostructure patterns as disparate as geometric characterization of ear [25], of iris [26], of the eye as a multimodal biometric system [27] and of the distribution of veins in a finger [28] or on the wrist [29].

However, in the 21st-century particular attention must be paid to the use of biological signals like biometric markers, in addition to morphological and behavioral characteristics. In this regard, worth highlighting biometrics studies involving the analysis of electrocardiographic (ECG) and encephalographic (EEG) signals [30], to which could be added biometric applications that obtain the biological signals from the galvanic response of skin (GSR), electromyogram (EMG), electrooculography (EOG), and mechanomyogram (MMG), among others [31].

Over the years, technological advances have simplified the acquisition of biological data; somehow, *traditional biometric systems* (TBS) have been increasingly giving way to *wearable biometric systems* (WBS), and, thus, to new methodological approaches to computing and validating biometric patterns [32]. Accordingly, new biometric technologies are gradually abandoning the rigidity imposed by a stationary and static analysis of biometric patterns [33] towards biometric patterns adapted to the variations that the biological signals may undergo over time—the so-called *adaptive biometric systems* [34]—. In the particular case of the photoplethysmographic (PPG) signal, biometric patterns are strongly conditioned to physiological alterations, such as physical activity, emotional states, and time intervals in which measurements do. An apart from the impact of the different noise sources coupled in the PPG signal acquisition procedure [11], mainly when the PPG signal is obtained from a camera or of wrist-worn PPG collected in an ambulant environment [35].

Focussing now on the matter at hand, the first documented reference to the PPG-based biometric system dates back to the research work of Gu *et al.* in 2003 [36]. In all the works that use the PPG signal as a biometric reference, specific biomarkers correspond to features implicitly or explicitly extracted from the signal waveform. For example, time-domain features acquired from PPG signal’s first and second derivatives for biometric identification [37], or approximating each PPG signal as a sum of Gaussians, and using the parameters in a discriminant analysis framework to distinguish individuals [38], or also defining the waveform of the PPG signal in five consecutive PPG cycles [39] or from 22 cycles [40] parametrically. One of the latest work is related to the non-fiducial and fiducial approaches for feature extraction with supervised and unsupervised machine learning classification techniques [41]. Other on the simultaneous PPG signal acquisition using different wavelengths thanks to the video camera detectors that allow extracting the color segment (e.g., red, green, and blue) [42]. In all PPG-based biometric models, an adverse aspect is the nature non-stationary of the PPG signal over time, which prevents the stable identification of an individual’s biometric patterns.

In this work, we moved away from the morphological analysis of the PPG signal to extract an individual’s biomarkers, and we now concentrate attention on its diffusive dynamic behavior, geometrically mapping on a 2D plane—do not be confused with extracting the PPG signal from an image [43] or remote sensing—, according to the theoretical approach introduced by the 0–1 test [44], as advanced in Section 1. Our proposal arises from the study carried out in the national research project [18, 19] wherein different biological signals of 40 individuals are analyzed, in one basal session and other with induced stress, using standard convolutional neural networks [45]. In light of preliminary findings, biometric patterns obtained through our PPG-based biometric system show promising stability to changes in the individual’s emotional state and the time lag, about one month, between samples of the PPG signal collected, unlike it can see in [38]. Future work will estimate the validation time of the biometric parameters obtained by examining the PPG signal’s diffusive dynamic behavior.

3 0–1 test

In the analysis of dynamic systems, one of the key aspects is to characterize the dynamic behavior present in the response of the physical system under study. The dynamics of the response, as such, does not provide direct relevant information on the internal physical structure from which the response derives. Still, it does provide at least its operational complexity, which is crucial in evaluating its correct functioning and its more or less adaptability to unforeseen situations in the context of physiological systems.

In an experimental setting, observables usually get from the physical system under consideration in such a way that the observables make measurements at regular time intervals. An observable is any physical quantity that can be measured. The measurements or observations organize in what is known as time sequences, and then each observable gives rise to a scalar time sequence. These temporal successions are submitted to the pertinent scrutiny to unravel the system’s functionality that generated them. We could define a state vector in phase space if we were able to measure all the observables that contribute to the dynamic evolution of a given system. In the field of physiological systems, it is widespread to work with univariate temporal sequences or scalar temporal sequences, in which only the measurements of an observable are available. With a single observable it is possible to obtain information on the state of the system, since each of them usually contains information from the others, given the mutual coupling between them, whether linear or non-linear.

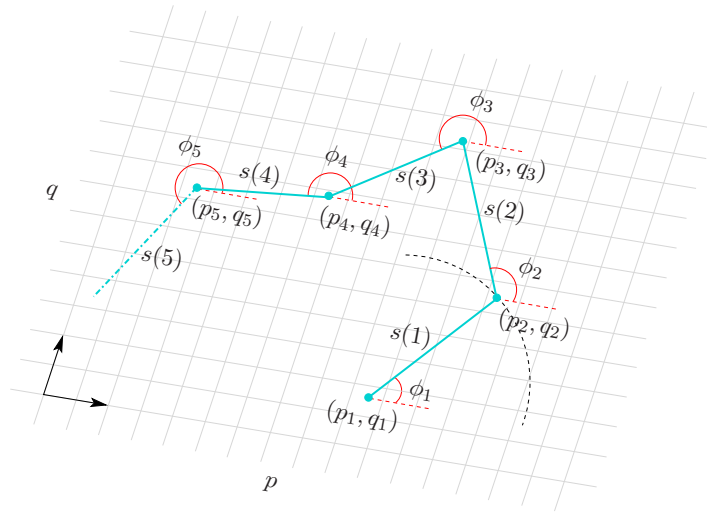


Figure 1: Descriptive construction of the auxiliary trajectory in the (p, q) -plane.

The initial motivation for the 0–1 test was to have a method to apply directly to a scalar temporal sequence to identify the presence of chaotic dynamics without having to resort to other more complicated techniques that require a deep level of knowledge for its correct application and interpretation [15, 16, 46]. Given its easy implementation, its increasing popularity has sparked the interest of countless scientific disciplines in an excessive race to detect chaos anywhere [17]. However, beyond the initial scope of the 0–1 test and its many applications, we believe that one of the phases of the test is surprisingly useful in the field of biometrics; specifically, the auxiliary trajectory of the two-dimensional Euclidean group (*the Fourier transform series*), or p - q diagram or (p, q) -plane [47], which underlies the dynamics of the physical system.

The 0–1 test cornerstone construction of an extended dynamic that serves a two-dimensional Euclidean group $\mathbf{SE}(2)$ [47]. The elements of $\mathbf{SE}(2)$ form rigid displacements, that is, a translation and a rotation, in some two-dimensional affine Euclidean plane—the (p, q) -plane—that, in principle, it does not relate in topological terms to the state space in which the dynamics of the system unfold. However, parameters that characterize rigid transformations depend at all times on the current state of the system and, therefore, a certain equivalence relationship manifest between the dynamics of the physical system under study and the dynamic evolution that the trajectory described by the elements of $\mathbf{SE}(2)$ in the (p, q) -plane.

The 0–1 test requires as input a scalar time sequence of N observations $s(n)$, for $n = 1, 2, \dots, N$, where $s(n)$ is a one-dimensional observable of the underlying dynamic system. The extension of the dynamics characterizes by $s(n)$ forces to define three scalar quantities (p, q, ϕ) according to the rigid transformations’ parameterization. An element or

point on the (p, q) -plane characterize by its position on the plane, whose coordinates are (p, q) , although its evolution, a change in coordinates, is driven (*forcing term*) by the dynamic evolution of $s(n)$ according to

$$\begin{aligned} p_{n+1} &= p_n + s(n) \cos \phi_n, \\ q_{n+1} &= q_n + s(n) \sin \phi_n, \\ \phi_{n+1} &= c + \alpha s(n), \end{aligned} \tag{1}$$

where parameters $c, \alpha \in \mathbb{R}$.

The evolution of any point on the (p, q) -plane describes a trajectory called the auxiliary trajectory since it reproduces an indirect or complementary evolution of the true dynamics observed in the system. The auxiliary trajectory involves an angular rotation ϕ_n with respect to a circumference of radius $s(n)$ centered on the point (p_n, q_n) , as shown in Fig. 1.

Somehow the auxiliary trajectory derives from a diffusive process in which the diffusion dynamics are forced or driven by the s_n observations. In the presence of noise, for dynamic simplicity, α usually assigns a value of 0 [16, 46] so that Eq. (1) reformulates as

$$\begin{aligned} p_n &= \sum_{k=1}^n s(k) \cos(kc), \\ q_n &= \sum_{k=1}^n s(k) \sin(kc), \\ \phi_n &= cn, \end{aligned} \tag{2}$$

where the angle of rotation ϕ_n increases at a uniform rate governed by the value of c . Furthermore, since the parameter c participates in the trigonometric functions argument, it is pertinent that $c \in [0, 2\pi)$.

Although the theory underlying the dynamic extensions is based on the asymptotic behavior of the dynamics, an interesting consequence of this focuses attention on the limit nature of auxiliary trajectories in the (p, q) -plane. That is, how the auxiliary trajectory evolves spatially in the (p, q) -plane if the trajectory is circumscribed in an area delimited from the (p, q) -plane or inexorably diffuses by the *plane* (p, q) in the same way that a Brownian motion unfolds [46]. The test 0–1 quantifies by the computation of an indicator whether the auxiliary trajectory is bounded, in which case it reflects the presence of a regular dynamics, or not sublinearly bounded, in which case it manifests the presence of a chaotic dynamics. This inductive argument is the base of the 0–1 test, a more in-depth description goes beyond this article objective, readers are referred to this method’ original work, widely referred to in the scientific literature in the last decade [15, 16, 46, 48].

This article uses young and healthy individuals’ PPG signals -more precisely, the geometric configurations described by their auxiliary trajectories in the (p, q) -plane to identify individuals biometrically by considered convolutional neural networks. As already stated in another article [44], the dynamic richness of the auxiliary trajectories of the PPG signals, for a range of values of the parameter c that prevents the appearance of spurious phenomena, reveals the inherent functional complexity to signal dynamics, to which multiple conveniently coupled physiological subsystems contribute. The coordinated action of these subsystems is responsible for homeostatic regulation of the cardiorespiratory system at all times. However, despite the certain global similarity that the auxiliary trajectories of PPG signals may have at first glance, closer scrutiny of each individual shows distinctive signs that could hide more or less serious diagnostic pathologies, and, more invariably, the inalienable character of the anatomical and functional configuration of the cardiorespiratory system of each subject. Future work in this line could yield promising results. The approach presented here uses the dynamic analysis of diffusive processes provided by the 0–1 test, the diffusive geometry represented in the (p, q) -plane, as an additional pre-processing layer. This layer allows the PPG signals acquired in the time domain to convert into geometric maps according to the (p, q) -planes of the input PPG signals. The data used to train and evaluate the neural network address the PPG signals of 40 young and healthy individuals from a national study [18, 19]. The neural network uses the geometric maps of each individual to establish the similarity or divergence between different subjects and could validate or deny an input user’s identity to the identities stored and authorized by the authentication system. On the other hand, this article also examines the proposed method’s reliability and performance following current biometric standards. As far as we know, diffusive dynamics, the cornerstone of the 0–1 test, of a biological signal have never used to extract biometric characteristics, which gives this work a new operational perspective in the field of physiological biometrics.

4 Classifier

In this article, we propose an approach based on convolutional neural networks to identify users through their PPG signals, so that it is possible to know if two different PPG signals correspond to the same user. The system proposed here receives two-time segments of PPG signals, 1,000 points on each, as inputs, of which the first will be the standard segment and the second the segment of the user to compare. The system delivers as output a matching score normalized to the interval $[0, 1]$, which defines the degree of agreement between the two incoming PPG segments, namely, if the two input segments belong to the same user, matching score closer to 1, or not, matching score closer to 0. As far as the authors know, no other study considers the design of a biometric system using the diffusive dynamic information of a biological signal, according to the (p, q) -planes provided by a preliminary phase of the 0–1 test. In the form of binary images, its output patterns feed a convolutional neural network that subsequently identifies the incoming users concerning those already registered. On the other hand, other studies try to solve the biometrics problem from other points of view in the PPG signal [37, 38, 40] and through other types of biological patterns [27, 24, 28, 25, 21, 49, 50].

4.1 Architecture

This article proposes a non-conventional network, as we can see in Fig. 2, whose main architecture base on a Siamese network whose main trunk is characterized by a fully-connected encoder, a multiscale architecture with residual connections based on the guidelines of Szegedy *et al.* [51]. Fully connected encoder architectures are those traditionally used in classification tasks such as [52, 53]. In the Siamese configuration case, this is well-known for its use in one-shot learning and image verification [54]. In addition to these layers and architectures somewhat better known in the field, the addition of a layer of its own to the system, which performs pre-processing based on the diffusive behavior peculiar to the PPG signal dynamics [44], is highlighted as a new contribution to this article.

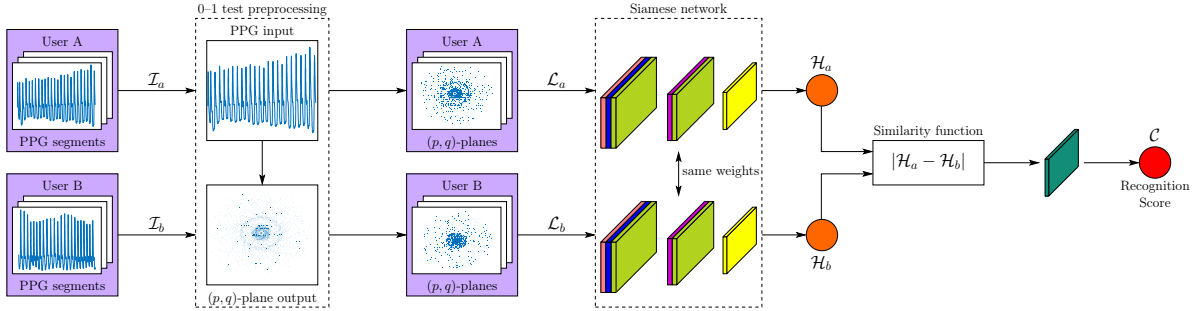


Figure 2: System’s architecture schematic overview.

The reason for using Inception-ResNet-V1 [51] architecture as the main branch of the Siamese network is due to its well-known capacity as a classifier and its characteristics concerning its previous versions and competing networks:

- Reduction of architectural bottlenecks for [55, 56], because the neural network works better if the dimensional input changes are not too drastic. Large dimensional changes can cause great loss of information, is what is called a “representational bottleneck”.
- Use of factoring methods to reduce the computational complexity of the convolutions used.
- Use of residual connections between the inputs and outputs of the blocks used. These connections prevent the loss of information and improve the stability of the gradients when training.
- Use of batch normalization to immunize the network to some extent against changes of scale, reduce training time, and avoid displacement of covariance.

The basic structure of the proposed system takes the form of a network combining 1D information (PPG signals) and 2D information ((p, q) -planes of PPG segments). This structure contains two distinct phases. The first phase consists of a pre-processing layer based on the characteristic (p, q) -planes of the 0–1 test. This phase will have as input six segments of the PPG signal from two users, three belonging to a registered user $\mathcal{P}_{r1}, \mathcal{P}_{r2}, \mathcal{P}_{r3}$, and the rest to a candidate user $\mathcal{P}_{c1}, \mathcal{P}_{c2}, \mathcal{P}_{c3}$, not necessarily different. Once these signal segments enter the 0–1 test pre-processing layer, their signals are featurized with this process and six output matrices are obtained $\mathcal{I}_{r1}, \mathcal{I}_{r2}, \mathcal{I}_{r3}$, and $\mathcal{I}_{c1}, \mathcal{I}_{c2}, \mathcal{I}_{c3}$, which can be represented as an image $\mathcal{I} = [\mathcal{I}_1, \mathcal{I}_2, \mathcal{I}_3]$, which represent the patterns corresponding to the PPG signals of those users.

The second phase will use as input these six output matrices obtained in the previous phase, in two matrices with three channels each, since each user has three matrices assigned to him. This phase consists of a Siamese network whose

architecture base on [51]. This network will use a single coding branch to process the two input matrices separately, that is, with the same trunk and sharing the same weights, some coded output features \mathcal{F}_r and \mathcal{F}_c will be obtained for each of the input matrices. Once features obtain, a relation function of these characteristics uses to quantify the error between them and quantify how similar these users are to each other. This error function represents the L^1 -norm between the vectors of characteristics previously obtained. Once the L^1 -norm standard obtain between the characteristics vectors, these will go through a final fully connected binary classification layer, in which a sigmoidal activation used to obtain a final \mathcal{C} score between 0 and 1, which quantifies how similar or different the evaluated users are. The architecture can observe in detail in Table 1.

Table 1: Proposed CNN detailed architecture. All the sub-blocks that belongs to the original Inception-ResNet architecture can be found in the seminal paper [51].

Layer number	Type	Output size	Configuration
1 _A	Input	(1000, 3)	—
1 _B	Input	(1000, 3)	—
2	0–1 test preprocessing	$2 \cdot (299, 299, 3)$	Siamese
3	Stem	$2 \cdot (35, 35, 256)$	Siamese
4	$5 \times$ Inception-ResNet-A	$2 \cdot (35, 35, 256)$	Siamese
5	Reduction-A	$2 \cdot (17, 17, 896)$	Siamese
6	$10 \times$ Inception-Resnet-B	$2 \cdot (17, 17, 896)$	Siamese
7	Reduction-B	$2 \cdot (8, 8, 1792)$	Siamese
8	$5 \times$ Inception-Resnet-C	$2 \cdot (8, 8, 1792)$	Siamese
9	Similarity function	(8, 8, 1792)	—
11	Flatten	114688	—
12	Dense	1	—
13	Sigmoidal activation	1	—

4.2 Training

In this section, we will proceed to explain the training. The first thing that needs to be explained is that to train 40 real-world PPG signals from different individuals obtained through a national research study used [18, 19]. In this step, we train the neural network with data from real-world biological signals, which we will divide into training, validation, and test sets, composed of 60%, 20%, and 20%, respectively, of the data from the database. These division ranges commonly chosen to ensure that almost half of the data used for evaluation. The training parameters explain below.

4.2.1 Optimizer

The optimizer used is *Adam* or Adaptive Moment Estimation [57]. This optimizer is a great alternative to the conventional Stochastic Gradient Descent (SGD), and combines the advantages of two previous alternatives [58, 59], creating a new approach that uses the averages of the first and second moments of the gradient to adapt the learning rate dynamically. When we talk about the learning rate, we refer to the parameters that define how much and how fast the system learns in each period. This parameter is crucial and can produce great learning problems if it does not choose correctly. A very high learning rate can produce divergence in training, while a very low rate can easily fall into local training minima or take a long time to complete. When we talk about *Adam*'s adaptive capabilities, we mean that in practical terms it starts with a user-defined learning rate, but after that, it modifies the learning rate through unsupervised training, this allows the use of an adaptive training ratio, but that depends strongly on the batch size and how noisy the input is. The training ratio initially used is 10^{-4} . In addition to *Adam*'s functionality, a callback called

early stopping has been employed in this training, this tool allows the best weight settings to save that the system has achieved throughout the training. In order to achieve this, the tool uses the metrics and losses obtained by the model in each period, so that it can save only the best model of all the periods trained—the network trained during 100 epochs with a batch size of 5. However, a predefined number of epochs used, as we have commented before, the early stopping will keep the best of them. The total training time, on a GPU NVIDIA GeForce GTX 1080, has been of 9 hours.

4.2.2 Loss function

The proposed convolutional neural network uses as input two PPG signal segments \mathcal{I}_a and \mathcal{I}_b , while as output, it uses a binary classification vector \mathcal{C} . The proposed loss function for this binary classification task is the cross-entropy (CE), as indicated in Eq. (3), which evaluates the differences between *Ground Truth* and predictions to provide an output score associated with the similarity of the input signals. In classical machine learning, this loss function has been widely used to solve the problems associated with a binary classification between distributions, being $p(x)$ the correct distribution and $q(x)$ the estimated one, so that it allows to associate a similarity score for those distributions.

$$\text{CE}(p, q) = - \sum_{\forall x} p(x) \log(q(x)). \quad (3)$$

Binary cross-entropy measures the classifier’s capacity under study, whose output is a classification level that associates the input to the distribution of interest. The more this classification level decreases, the more the cross-entropy losses increase. The perfect classifier would have zero cross-entropy with a maximum classification level. Usually, this loss function is used in neural networks accompanied by an output activation according to it. In binary cross-entropy, activation is sigmoid, which places the output score level in the interval $[0, 1]$, with a smooth transition.

Finally, we will explain step by step how the training of the neural network takes place. The problem to be solved by this system is a binary classification problem with only two possible classes, class 0, which indicates that the input PPG segments of branch A and branch B do not belong to the same user, and class 1, which indicates that these segments belong to the same user. Each of the predefined training segments generated with a specific output label links these input segments A and B to an output classification, allowing the system to learn how to differentiate or associate the input segments of different users. Once in the training process, a random batch generator will use allowing choose 3 PPG signal segments belonging to user A from among the 40 PPG signals used and another 3 PPG signal segments belonging to user B, once again randomized, so that if these two users coincide an output label will be applying with class 1, while if not, it will be associated with class 0. This generator allows guaranteeing the highest possible variability, greatly enriching the training and providing it with generality. Once the batches generate, the *Adam* optimizer is used to train the system in the task of recognizing similar users. It is necessary to emphasize that the division of data between the set of training, validation and test has been of a 60% for training data and a 40% for validation and test data. After training, this system will be evaluated on the previously defined test sets, configured in different ways, as explained in the following sections. Each of these operating modes may require retraining of the system so that a correct ablation study can carry out to guarantee the proper functioning and conditions of this operation in different operative situations or work regimes.

5 Results

In this section, we show the biometric potential of the diffusive dynamics of the PPG signal. To do this, we explore its operational feasibility under different experimental conditions to mimic its effectiveness in possible real-life scenarios.

5.1 Preprocessing

In practice, the PPG signal is usually impaired by many common noise sources during the signal acquisition process, such as motion artifacts, sensor movements, breathing, etc, as well as for the discretization error (truncation error) involved in normalizing the input signal amplitudes. A common and direct mechanism to mitigate the effect of noise is to submit the PPG signal to a bandpass filter. For filtered PPG signals, we use a Butterworth bandpass filter tuned to different cutoff frequencies. To examine the impact that this early pre-processing has on the learning and the final performances of the our biometric system, we study the following variations:

1. Raw data: in this first mode, the PPG signals are not pre-processed and are transferred directly, as they were acquired, to the 0–1 test pre-processing layer (see Fig. 2), where once segmented they convert to diffusive geometric maps.

2. Filtered data [0.1–8 Hz]: in this second mode, the PPG signals, before moving to the 0–1 test pre-processing layer, are filtered with a Butterworth bandpass filter with cutoff frequencies at 0.1 and 8 Hz, and the amplitudes are not normalized.
3. Filtered data [0.5–8 Hz]: in this third mode, the PPG signals, before moving to the 0–1 test pre-processing layer, are filtered with a Butterworth bandpass filter with cutoff frequencies at 0.5 and 8 Hz, and the amplitudes are not normalized.
4. Filtered data [0.5–8 Hz] and normalized: in the latter mode, the PPG signals, before moving to the 0–1 test pre-processing layer, are filtered with a Butterworth bandpass filter with cutoff frequencies at 0.5 and 8 Hz, and the amplitudes normalized to the $[0, 1]$ interval.

5.2 Metrics

Once the modalities in which the experimentation will carry out fixed, the metrics used to evaluate the proposed system’s performance are explained:

- **Precision-Recall curve.** The precision-recall curve depicts the precision vs. the sensitivity (recall) for different operating points (matching score or threshold values). The closer the curve is to the upper right corner (the area under the curve is closer to 1), the more precise and sensitive the system behaves. The accuracy evaluates how often the output is correct (positive). An accurate system is very finicky validating a legitimate user, i.e. in an accurate system it is unlikely that an intrusive user will be admitted as valid, but it is also possible that legitimate users will be rejected (false negatives). Sensitivity assesses how permissive the system is, i.e., in a highly sensitive system, it is very unlikely that a valid user will be rejected but it is also possible that unregistered users will be admitted as valid (false positives).
- **ROC (Receiver Operating Characteristic) curve.** The ROC curve depicts the sensitivity vs. FPR (false positive rate). The closer the curve is to the upper left corner (the area under the curve is closer to 1) the more sensitive the system behaves without increasing FPR. In short, the ROC curve graphically represents TPR (true positive rate) vs. FPR (false positive rate) for different operating points (matching score or threshold values).
- **F₁ score-Threshold curve.** The F₁ score-Threshold curve complements the information provided by the Precision-recall curve. F₁ score is a joint and overall metric that brings together the Precision and Recall values in a unique metric (precision and recall harmonic mean) that allows us to have an estimation of the stability of the system’s performance for different threshold values. In a stable and high-performance system, the range of threshold values for which the curve remains almost constant and close to 1 is virtually a flat line over the whole range.
- **Equal Error Rate (EER).** The equal error rate or crossover error rate (CER) is a metric concerning biometric authentication systems that determines a working threshold where FPR (false positive rate) and FNR (false negative rate) are the same. The point where these decision errors cross define the working point, and the lower the crossover rate, the higher the system’s accuracy. At the experimental level, EER is used as a metric to compare different biometric authentication techniques.

Usually, a high decision threshold identifies an accurate model with a very low FPR (false positive rate); a low threshold value indicates a high sensitivity (too permissive, with a very low FNR (false negative rate)). The precision-recall and ROC curves help us to find the equilibrium threshold. In our case, the criteria for selecting the optimal threshold comes from the EER, but the F1 score-Threshold curve tells us if variations of the optimal threshold upwards or downwards would dramatically affect the system performance. Based on the results we will see later, the equilibrium threshold of the precision-recall and ROC curves would not be so critical, as the stability of the system has a wide operating margin for a not insignificant range of working thresholds.

5.3 Experimental conditions

5.3.1 Leaving 40% of users out of training

In this first experiment, all the users’ results show, leaving 40% of them isolated completely from the training. This way, the network is trained with 24 users and tested with 16 users never seen before. This experiment allows us to completely isolate 16 users so that the network has never seen a similar pattern in the training phase. Therefore, the register of authorized users does not record the biometrics ID of the 16 users who keep out.

Fig. 3 shows the different EERs for all the input PPG signals modalities used (cf. § 5.1). For raw data and filtered data in the range of 0.1 to 8 Hz, the network’s discriminating power is penalized by the noise present in the signal, which

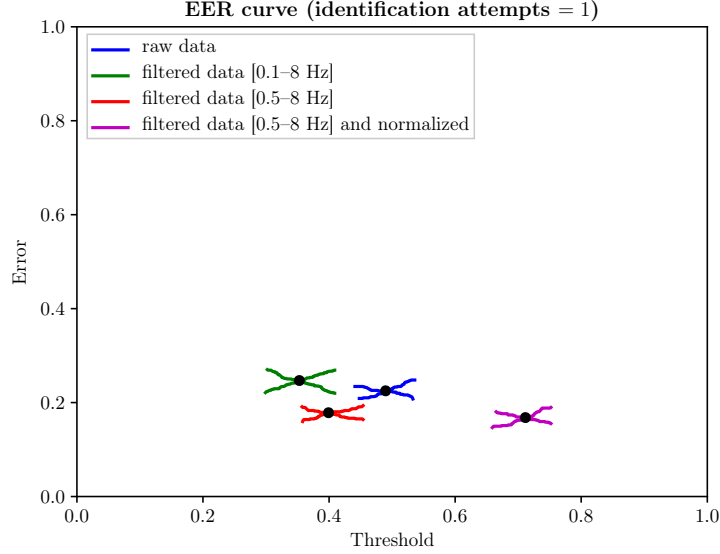


Figure 3: Equal Error Rate (EER) for different pre-processing modalities of the input PPG signal.

distorts and blurs the diffusive geometrical patterns in the (p, q) -planes. As filtering narrows its bandpass, in the range of 0.5 to 8 Hz, the noise reduction reduced, and the diffusive geometric pattern becomes clearer, allowing the network to discriminate between biometric patterns of different users more easily. If, besides, the PPG signal is normalized to the $[0, 1]$ interval, once filtered in the range of 0.5 to 8 Hz, a slight reduction in EER is seen. This effect is because the signal’s normalization improves the numerical quantification, and the diffusive geometric patterns trace a better structural resolution, making it easier to extract the biometric features.

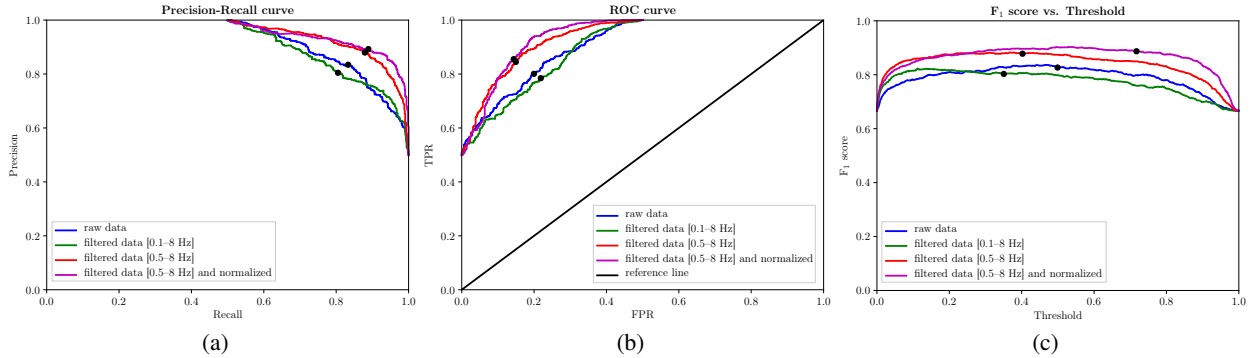


Figure 4: Functional efficiency curves in case leaving 40% of users out of training. The working points of the EER curve (see Fig. 3) are tagged with the symbol •: (a) Precision-Recall curve; (b) ROC curve; (c) F_1 score-Threshold curve.

From the EER curve can be measured the working points for each of the pre-processing modes. These working points can use to obtain other performance measures, as shown in Figs. 4a-4c. It can be seen that for raw data and filtered data in the range of 0.1 to 8 Hz, the functional efficiency curves, that is, Precision-Recall, ROC and F_1 score-Threshold curves, behave quite similarly. However, as illustrated in Figs. 4a-4c, the filtering in the range of 0.5 to 8 Hz provides a significant enhancement in system operating performance, especially about the stability of the working point, pointed out by the F_1 score-Threshold curve, much higher than the raw data and filtered data in the range of 0.1 to 8 Hz. Unlike in terms of EER curve in functional efficiency curves, the benefit of normalization to the $[0, 1]$ interval, once filtering the data in the range of 0.5 to 8 Hz, is remarkable. On the one hand, there is a marked improvement in performance for high thresholds, and, on the other hand, in the F_1 score-Threshold curve, the working point is much more stable than in any of the other modes.

Table 2 shows the performance metrics of the experiment whereby 40% of users are left out of training.

Table 2: Performance metrics for all the input PPG signals modalities used in case leaving 40% of users out of training. The thresholds refer to the optimal classification thresholds where EER is minimal for each modality (pre-processing) considered.

RAW DATA				
Precision	Recall	F ₁ score	Threshold	Equal Error Rate (EER)
0.82	0.82	0.82	0.48	0.22
FILTERED DATA [0.1–8 Hz]				
Precision	Recall	F ₁ score	Threshold	Equal Error Rate (EER)
0.80	0.80	0.80	0.37	0.23
FILTERED DATA [0.5–8 Hz]				
Precision	Recall	F ₁ score	Threshold	Equal Error Rate (EER)
0.89	0.89	0.89	0.40	0.19
FILTERED DATA [0.5–8 Hz] AND NORMALIZED IN [0, 1] INTERVAL				
Precision	Recall	F ₁ score	Threshold	Equal Error Rate (EER)
0.90	0.90	0.90	0.73	0.18

5.3.2 Leaving 40% of data out of training

In this second experiment, all the users’ results shown but using 60% of the total data as the training set, covering all the users, and a test set with the remaining 40% of data. Meaning that the network handles (p, q) -planes for all users in the training phase, but in a different way than they will be treated for testing, even though they are undoubtedly related to the specific users’ biometric patterns.

This experimental framework sets out a particular setting in which the registered users’ database already known, and therefore, no new user enrollments will occur. All users are well-known to the network since they have enrolled previously.

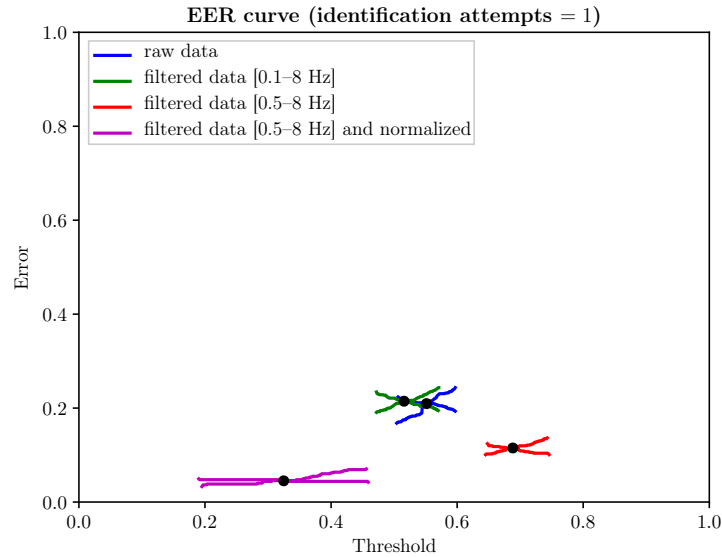


Figure 5: Equal Error Rate (EER) for different pre-processing modalities of the input PPG signal.

Fig. 5 shows the different EERs for all the input PPG signals modalities used (cf. § 5.1). For raw data and filtered data in the range of 0.1 to 8 Hz, the discriminating power of the network is similar to that obtained in the preceding

experimental framework (cf. § 5.3.1, Fig. 3). The noise present in the signal, which distorts and blurs the diffusive geometrical patterns in the (p, q) -planes, is a critical constraint on the biometrics system’s operational capability.

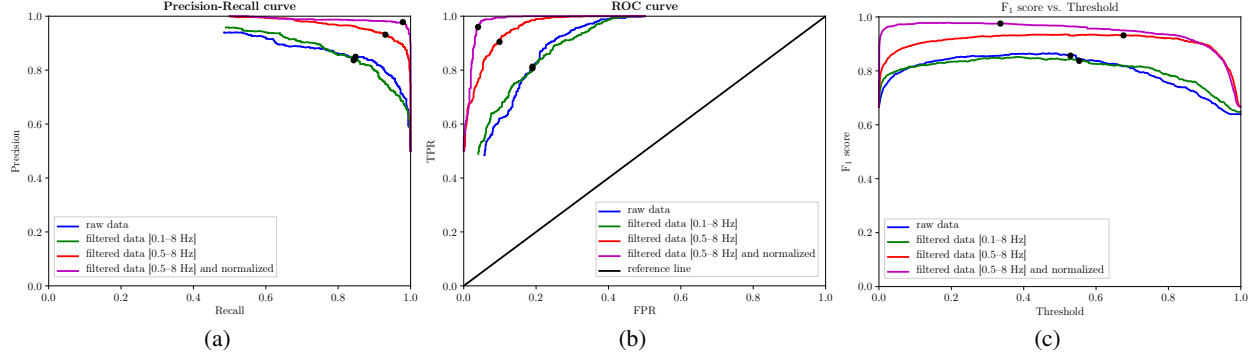


Figure 6: Functional efficiency curves in case leaving 40% of data out of training. The working points of the EER curve (see Fig. 5) are tagged with the symbol •: (a) Precision-Recall curve; (b) ROC curve; (c) F_1 score-Threshold curve.

Nevertheless, contrary to what appears in Fig. 3, for filtering in the range of 0.5 to 8 Hz, the network offers high efficiency, with a significant reduction of EER. If, besides, the PPG signal is normalized to the $[0, 1]$ interval, once filtered in the range of 0.5 to 8 Hz, the least EER is reached, very close to zero (6%, as indicated in Table 3). With such credentials, it is already clear how a properly pre-processing of the input PPG signals can positively influence the final throughput of the biometric system.

From the EER curve can be measured the working points for each of the pre-processing modes. These working points can use to obtain other performance measures, as shown in Figs. 6a-6c. It can be seen that for raw data and filtered data in the range of 0.1 to 8 Hz, the functional efficiency curves, that is, Precision-Recall, ROC and F_1 score-Threshold curves, behave almost equally for classification purposes. Otherwise, when filtering in the range of 0.5 to 8 Hz is applied to the input data, a qualitative leap is obtained in terms of operational performance, notably about the smooth stability of the F_1 score-Threshold curve (see Fig. 6c). Additionally, the fact of normalizing the data to $[0, 1]$ interval, once filtering the data in the range of 0.5 to 8 Hz, enables the network to operate as an quasi-optimal classifier, with behavior similar to a perfect classifier.

Table 3: Performance metrics for all the input PPG signals modalities used in case leaving 40% of data out of training. The thresholds refer to the optimal classification thresholds where EER is minimal for each modality (pre-processing) considered.

RAW DATA				
Precision	Recall	F_1 score	Threshold	Equal Error Rate (EER)
0.86	0.86	0.86	0.53	0.21
FILTERED DATA [0.1–8 Hz]				
Precision	Recall	F_1 score	Threshold	Equal Error Rate (EER)
0.82	0.82	0.82	0.57	0.22
FILTERED DATA [0.5–8 Hz]				
Precision	Recall	F_1 score	Threshold	Equal Error Rate (EER)
0.93	0.93	0.93	0.68	0.11
FILTERED DATA [0.5–8 Hz] AND NORMALIZED IN $[0, 1]$ INTERVAL				
Precision	Recall	F_1 score	Threshold	Equal Error Rate (EER)
0.97	0.97	0.97	0.34	0.06

Table 3 shows the performance metrics of the experiment whereby 40% of data are left out of training. Finally, we also compare in Table 4 performance metrics with other PPG-based biometric methods, in order to consolidate the potential viability attributable to our biometric authentication system. Ratings shown in Table 4 are merely indicative and are limited to the achievements obtained in different experimental scenarios and with different databases. Unfortunately, there is no common roadmap available for the different PPG-based methods to provide the results obtained. However, always with the utmost respect for the work carried out by authors, we chose to report the best performances when there is not enough information available to conduct a comparison that is as fair as possible on equal terms.

As Spachos *et al.* noted [39], the performance of PPG signal acquisition equipment and the environmental conditions when acquiring the signals has a substantial impact on the operational feasibility of any biometric authentication system. So far, most PPG-based biometric systems, as listed in Table 4, extract the representative features of a individual from the morphology of the PPG signal, either directly from the acquired PPG signal itself or with time or frequency domain transformations. Accordingly, the vulnerability of the morphology of the PPG signal to the physical state of the subject, and to the environmental and instrumental conditions in the signal acquisition process, restrict its field of application to biometric environments where very stable conditions are guaranteed, namely, when PPG signals, in enrollment and testing phases, were collected under controlled environment and with accurate sensors.

Table 4: Comparison of performances for PPG-based recognition of state-of-the-art methods. Claimed error rates (EERs) involve that in the trial, three attempts were allowed. Average comparison time refers to the time spent by the system to identify whether the user is valid or not.

PPG-based biometric recognition method	Equal Error Rate (EER) (%)	Rank-1 accuracy (%)	Average comparison time (s)
Sancho <i>et al.</i> 2018 [1]	6.9	—	0.25
Patil <i>et al.</i> 2018 [42]	23.34	86.67	—
Yadav <i>et al.</i> 2018 [11]	0.5	—	—
Karimian <i>et al.</i> 2017 [41]	1.31	99.84	—
Sarkar <i>et al.</i> 2016 [38]	—	90.53	—
Lee and Kim 2015 [40]	3.7	96.80	—
Kavsaoğlu <i>et al.</i> 2014 [37]	—	94.44	—
Spachos <i>et al.</i> 2011 [39]	0.5	—	—
Our approach	2.0	97.0	0.01

In the light of the above, the inherent biometric limitations of PPG signal morphology are not reflected in the methods collected in Table 4, where an in-depth analysis reveals the high variability being experienced by the parameter EER, degrading its expectations, a priori of the most promising, when PPG signals are acquired under different conditions. So, in Sancho *et al.* [1] the range of percentage variation of EER is 13.9 (from 6.9 to 20.8%) when evaluated on different time-lapses, in Yadav *et al.* [11] it is 5.5 (from 0.5 to 6%) when evaluated on different states and datasets, or in Spachos *et al.* [39] it is 24.5 (from 0.5 to 25%) when evaluated on different datasets. In the other methods, only the method’s potential is evaluated focusing on the research approach, rather than as a feasible real biometric solution, such as in Karimian *et al.* [41], where the proposed solution provides very good performances, with Error Rate and rank-1 accuracy of 1.31% y 99.84%, respectively, but in principle 8 minutes of PPG signal are required, against the 12 seconds of our approach. Either way, exogenous and endogenous factors in the PPG signal’s morphological fluctuations may discourage its use in wearable biometric systems, as consistent and reliable results with reasonable operations could not be guaranteed.

The present proposal instead provides the opportunity to open up a new line of work in PPG- based biometry. The analysis of the morphology of the PPG signal is now replaced by the study of its diffusive dynamics, our (p, q) -planes, highly dependent on the biostructure of vascular bed, an intricate network of tiny blood vessels that ramifies through the tissues of the body. While deteriorating with age and/or with certain cardiovascular diseases, this vascular microstructure is unique to each individual and maintains a reasonably regular and stable diffusive conductivity over time, which makes this an excellent biometric marker. In fact, preliminary trials with our biometric authentication system yielded similar performance ratings, with EER and rank-1 accuracy, with one attempt, in the range of about 6% and 97%, respectively, when users, initially registered in a relaxed state, were successfully identified about 30 days later under stress-induced conditions.

With an enrollment time of 12 s, we truly believe that our technical approach has the potential to become a real low-cost technological solution, built-in in miniaturized Tensor Processing Units (TPUs) customized for a particular use in

wearable biometric systems, since once the network has been suitably trained, the authentication methodology does not require successive retraining for reliable serving. Moreover, the memory requirements for storing users' biometric templates, is around of 120 kB, pose no apparent constraints on the portable logistics of the authorized user database. Efforts are being made to reduce PPG signals acquisition time, more in step with the average comparison time, about 10 ms, in verifying biometric credentials of a user requesting access to the system.

6 Conclusions

Over the past 10 years, the easily accessible PPG signal has attracted the attention of those involved in biometric security. Most PPG-based biometric solutions define the biometric signature of a user out of certain features of the PPG signal morphology. Yet, the high variability of the PPG signal morphology, in reaction to changes in measurement conditions and the psychophysical state of the individual, is hampering its adoption as a biometric solution in wearable systems.

In this research work, still in progress, we propose a robust PPG-based biometric authentication system on the basis of the diffusive dynamics of the PPG signal, arguably very stable in changing environments, instead of morphological aspects of the signal. Our biometrics approach is based upon convolutional neural networks, easily integrated into embedded environments, that can reach high speeds in the identification process. Error rates and rank-1 accuracy, with one attempt, in the range of about 6% and 97%, respectively, indicate significance and potential viability as a biometric candidate. Future work involves expanding the dataset with different physiological conditions, but some preliminary results with the same individuals under stress conditions, and at two different time spans, suggest a promising operational consistency in the authentication process.

Acknowledgments

The authors would like to thank Life Supporting Technologies Group (LST-UPM) for taking part in project FIS-PII2/00514, from MINECO.

References

- [1] Jorge Sancho, Álvaro Alesanco, and José García. Biometric authentication using the PPG: A long-term feasibility study. *Sensors*, 18(5):1525, may 2018.
- [2] R. Sanchez-Reillo, C. Sanchez-Avila, and A. Gonzalez-Marcos. Biometric identification through hand geometry measurements. *IEEE Transactions on Pattern Analysis and Machine Intelligence*, 22(10):1168–1171, 2000.
- [3] Jermama Moraes, Matheus Rocha, Glauber Vasconcelos, José Vasconcelos Filho, Victor de Albuquerque, and Auzuir Alexandria. Advances in photoplethysmography signal analysis for biomedical applications. *Sensors*, 18(6):1894, jun 2018.
- [4] Mohamed Elgendi. Standard terminologies for photoplethysmogram signals. *Current Cardiology Reviews*, 8(3):215–219, sep 2012.
- [5] A. B. Hertzman. Photoelectric plethysmography of the fingers and toes in man. *Experimental Biology and Medicine*, 37(3):529–534, dec 1937.
- [6] Denisse Castaneda, Aibhlin Esparza, Mohammad Ghamari, Cinna Soltanpur, and Homer Nazeran. A review on wearable photoplethysmography sensors and their potential future applications in health care. *International Journal of Biosensors & Bioelectronics*, 4(4):195–202, 2018.
- [7] Daniel J. Peart, Carlos Balsalobre-Fernández, and Matthew P. Shaw. Use of mobile applications to collect data in sport, health, and exercise science: A narrative review. *Journal of Strength and Conditioning Research*, page 1, aug 2018.
- [8] John Allen. Photoplethysmography and its application in clinical physiological measurement. *Physiological Measurement*, 28(3):R1–R39, feb 2007.
- [9] Mohamed Elgendi. On the analysis of fingertip photoplethysmogram signals. *Current Cardiology Reviews*, 8(1):14–25, jun 2012.
- [10] Nina Sviridova and Kenshi Sakai. Application of photoplethysmogram for detecting physiological effects of tractor noise. *Engineering in Agriculture, Environment and Food*, 8(4):313–317, oct 2015.
- [11] Umang Yadav, Sherif N. Abbas, and Dimitrios Hatzinakos. Evaluation of PPG biometrics for authentication in different states. In *2018 International Conference on Biometrics (ICB)*. IEEE, feb 2018.

- [12] J. G. Webster. *Design of Pulse Oximeters*. Series in Medical Physics and Biomedical Engineering. CRC Press, 1997.
- [13] S. Dhar, S.K. Mukhopadhyay, S. Pal, and M. Mitra. An efficient data compression and encryption technique for PPG signal. *Measurement*, 116:533–542, feb 2018.
- [14] D. J. Meredith, D. Clifton, P. Charlton, J. Brooks, C. W. Pugh, and L. Tarassenko. Photoplethysmographic derivation of respiratory rate: a review of relevant physiology. *Journal of Medical Engineering & Technology*, 36(1):1–7, dec 2011.
- [15] Georg A. Gottwald and Ian Melbourne. A new test for chaos in deterministic systems. *Proceedings of the Royal Society of London. Series A: Mathematical, Physical and Engineering Sciences*, 460(2042):603–611, feb 2004.
- [16] Georg A. Gottwald and Ian Melbourne. Testing for chaos in deterministic systems with noise. *Physica D: Nonlinear Phenomena*, 212(1-2):100–110, dec 2005.
- [17] Davide Bernardini and Grzegorz Litak. An overview of 0–1 test for chaos. *Journal of the Brazilian Society of Mechanical Sciences and Engineering*, 38(5):1433–1450, nov 2015.
- [18] Jordi Aguiló, Pau Ferrer-Salvans, Antonio García-Rozo, Antonio Armario, Ángel Corbi, Francisco J. Cambra, Raquel Bailón, Ana González-Marcos, Gerardo Caja, Sira Aguiló, Raúl López-Antón, Adriana Arza-Valdés, and Jorge M. Garzón-Rey. Project es3: attempting to quantify and measure the level of stress. *Revista de Neurología*, 61:405–415, nov 2015.
- [19] Adriana Arza, Jorge Mario Garzón-Rey, Jesús Lázaro, Eduardo Gil, Raúl López-Antón, Conchita de la Cámara, Pablo Laguna, Raquel Bailón, and Jordi Aguiló. Measuring acute stress response through physiological signals: towards a quantitative assessment of stress. *Medical & Biological Engineering & Computing*, 57(1):271–287, aug 2018.
- [20] Celia Paulsen and Robert Byers. Glossary of key information security terms. Technical report, Computer Security Division. Information Technology Laboratory. National Institute of Standards and Technology (NIST), jul 2019.
- [21] Hao Liu, Xiangyu Zhu, Zhen Lei, and Stan Z. Li. Adaptiveface: Adaptive margin and sampling for face recognition. In *The IEEE Conference on Computer Vision and Pattern Recognition (CVPR)*, June 2019.
- [22] Xuefei Yin, Yanming Zhu, and Jiankun Hu. 3d fingerprint recognition based on ridge-valley-guided 3d reconstruction and 3d topology polymer feature extraction. *IEEE Transactions on Pattern Analysis and Machine Intelligence*, pages 1–1, 2019.
- [23] A.K. Jain, A. Ross, and S. Prabhakar. An introduction to biometric recognition. *IEEE Transactions on Circuits and Systems for Video Technology*, 14(1):4–20, jan 2004.
- [24] S. Rajeev, K. K. M. Shreyas, K. Panetta, and S. Agaian. 3-d palmprint modeling for biometric verification. In *2017 IEEE International Symposium on Technologies for Homeland Security (HST)*, pages 1–6, 2017.
- [25] Jie Zhang, Wen Yu, Xudong Yang, and Fang Deng. Few-shot learning for ear recognition. In *Proceedings of the 2019 International Conference on Image, Video and Signal Processing, IVSP 2019*, page 50–54, New York, NY, USA, 2019. Association for Computing Machinery.
- [26] Kuo Wang and Ajay Kumar. Cross-spectral iris recognition using CNN and supervised discrete hashing. *Pattern Recognition*, 86:85–98, feb 2019.
- [27] S. N. Dharwadkar and R. P. Anant. Combining eye based features for biometric system. In *2015 International Conference on Information Processing (ICIP)*, pages 409–413, 2015.
- [28] C. Liu, S. Ruan, Y. Lai, and C. Yao. Finger-vein as a biometric-based authentication. *IEEE Consumer Electronics Magazine*, 8(6):29–34, 2019.
- [29] Raul Garcia-Martin and Raul Sanchez-Reillo. Vein biometric recognition on a smartphone. *IEEE Access*, 8:104801–104813, 2020.
- [30] Yogendra Narain Singh, Sanjay Kumar Singh, and Amit Kumar Ray. Bioelectrical signals as emerging biometrics: Issues and challenges. *ISRN Signal Processing*, 2012:1–13, 2012.
- [31] Anita Pal, Ajeet Kumar Gautam, and Yogendra Narain Singh. Evaluation of bioelectric signals for human recognition. *Procedia Computer Science*, 48:746–752, 2015.
- [32] Jorge Blasco, Thomas M. Chen, Juan Tapiador, and Pedro Peris-Lopez. A survey of wearable biometric recognition systems. *ACM Computing Surveys*, 49(3):1–35, dec 2016.
- [33] Chan-II Kim and Jong-Ha Lee. The non-contact biometric identified bio signal measurement sensor and algorithms. *Technology and Health Care*, 26(Papers from the 6th International Conference on Biomedical Engineering and Biotechnology (iCBEB2017), 17–20 October 2017, Guangzhou, China):215–228, May 2018.

- [34] Paulo Henrique Pisani, Abir Mhenni, Romain Giot, Estelle Cherrier, Norman Poh, André Carlos Ponce de Leon Ferreira de Carvalho, Christophe Rosenberger, and Najoua Essoukri Ben Amara. Adaptive biometric systems. *ACM Computing Surveys*, 52(5):1–38, sep 2019.
- [35] Dwaipayan Biswas, Luke Everson, Muqing Liu, Madhuri Panwar, Bram-Ernst Verhoef, Shrishail Patki, Chris H. Kim, Amit Acharyya, Chris Van Hoof, Mario Konijnenburg, and Nick Van Helleputte. CorNET: Deep learning framework for PPG-based heart rate estimation and biometric identification in ambulant environment. *IEEE Transactions on Biomedical Circuits and Systems*, 13(2):282–291, apr 2019.
- [36] Y.Y. Gu, Y. Zhang, and Y.T. Zhang. A novel biometric approach in human verification by photoplethysmographic signals. In *4th International IEEE EMBS Special Topic Conference on Information Technology Applications in Biomedicine, 2003*. IEEE, 2003.
- [37] A. Reşit Kavsaoğlu, Kemal Polat, and M. Recep Bozkurt. A novel feature ranking algorithm for biometric recognition with PPG signals. *Computers in Biology and Medicine*, 49:1–14, jun 2014.
- [38] Abhijit Sarkar, A. Lynn Abbott, and Zachary Doerzaph. Biometric authentication using photoplethysmography signals. In *2016 IEEE 8th International Conference on Biometrics Theory, Applications and Systems (BTAS)*. IEEE, sep 2016.
- [39] Petros Spachos, Jiexin Gao, and Dimitrios Hatzinakos. Feasibility study of photoplethysmographic signals for biometric identification. In *2011 17th International Conference on Digital Signal Processing (DSP)*. IEEE, jul 2011.
- [40] Anthony Lee and Younghyun Kim. Photoplethysmography as a form of biometric authentication. In *2015 IEEE SENSORS*. IEEE, nov 2015.
- [41] Nima Karimian, Mark Tehranipoor, and Domenic Forte. Non-fiducial PPG-based authentication for healthcare application. In *2017 IEEE EMBS International Conference on Biomedical & Health Informatics (BHI)*. IEEE, 2017.
- [42] Omkar R. Patil, Wei Wang, Yang Gao, Wenyao Xu, and Zhanpeng Jin. A non-contact PPG biometric system based on deep neural network. In *2018 IEEE 9th International Conference on Biometrics Theory, Applications and Systems (BTAS)*. IEEE, oct 2018.
- [43] Yu Sun and Nitish Thakor. Photoplethysmography revisited: From contact to noncontact, from point to imaging. *IEEE Transactions on Biomedical Engineering*, 63(3):463–477, mar 2016.
- [44] J. de Pedro-Carracedo, A.M. Ugena, and A.P. Gonzalez-Marcos. Dynamical analysis of biological signals with the 0–1 test. *arXiv.org*, preprint(arXiv:1906.00782):1–8, may 2019.
- [45] Raquel Ruíz Orozco. Diseño de redes convolucionales para la clasificación de imágenes médicas. Bachelor degree, ETSI Telecomunicación, Universidad Politécnica de Madrid (UPM), Madrid, Spain, 2019.
- [46] Georg A. Gottwald and Ian Melbourne. On the implementation of the 0–1 test for chaos. *SIAM Journal on Applied Dynamical Systems*, 8(1):129–145, jan 2009.
- [47] Matthew Nicol, Ian Melbourne, and Peter Ashwin. Euclidean extensions of dynamical systems. *Nonlinearity*, 14(2):275–300, jan 2001.
- [48] Georg A. Gottwald and Ian Melbourne. On the validity of the 0–1 test for chaos. *Nonlinearity*, 22(6):1367–1382, may 2009.
- [49] Ajay Kumar and Cyril Kwong. Towards contactless, low-cost and accurate 3d fingerprint identification. In *2013 IEEE Conference on Computer Vision and Pattern Recognition*. IEEE, jun 2013.
- [50] Jinxiu Liang, Jingwen Wang, Yuhui Quan, Tianyi Chen, Jiaying Liu, Haibin Ling, and Yong Xu. Recurrent exposure generation for low-light face detection. *arXiv.org*, preprint(arXiv:2007.10963):1–12, july 2020.
- [51] Christian Szegedy, Sergey Ioffe, Vincent Vanhoucke, and Alexander Alemi. Inception-v4, inception-resnet and the impact of residual connections on learning. *AAAI Conference on Artificial Intelligence*, 02 2016.
- [52] Karen Simonyan and Andrew Zisserman. Very deep convolutional networks for large-scale image recognition. In *International Conference on Learning Representations*, 2015.
- [53] Christian Szegedy, Wei Liu, Yangqing Jia, Pierre Sermanet, Scott Reed, Dragomir Anguelov, Dumitru Erhan, Vincent Vanhoucke, and Andrew Rabinovich. Going deeper with convolutions. In *2015 IEEE Conference on Computer Vision and Pattern Recognition (CVPR)*. IEEE, jun 2015.
- [54] Gregory R. Koch. Siamese neural networks for one-shot image recognition. In *Proceedings of the 32nd International Conference on Machine Learning*, Lille, France, 2015.

- [55] C. Szegedy, Wei Liu, Yangqing Jia, P. Sermanet, S. Reed, D. Anguelov, D. Erhan, V. Vanhoucke, and A. Rabinovich. Going deeper with convolutions. In *2015 IEEE Conference on Computer Vision and Pattern Recognition (CVPR)*, pages 1–9, 2015.
- [56] Christian Szegedy, Vincent Vanhoucke, Sergey Ioffe, Jonathon Shlens, and Zbigniew Wojna. Rethinking the inception architecture for computer vision. *CoRR*, abs/1512.00567, 2015.
- [57] Diederik Kingma and Jimmy Ba. Adam: A method for stochastic optimization. *International Conference on Learning Representations*, 12 2014.
- [58] John Duchi, Elad Hazan, and Yoram Singer. Adaptive subgradient methods for online learning and stochastic optimization. *Journal of Machine Learning Research*, 12:2121–2159, 07 2011.
- [59] Yann N. Dauphin, Harm de Vries, Junyoung Chung, and Yoshua Bengio. Rmsprop and equilibrated adaptive learning rates for non-convex optimization. *CoRR*, abs/1502.04390, 2015.